

Directional Filter Design and Simulation for Superconducting On-Chip Filter-Banks

Marting, Louis H.; Karatsu, Kenichi; Endo, Akira; Baselmans, Jochem J.A.; Pascual Laguna, Alejandro

DOI

[10.1007/s10909-024-03118-w](https://doi.org/10.1007/s10909-024-03118-w)

Publication date

2024

Document Version

Final published version

Published in

Journal of Low Temperature Physics

Citation (APA)

Marting, L. H., Karatsu, K., Endo, A., Baselmans, J. J. A., & Pascual Laguna, A. (2024). Directional Filter Design and Simulation for Superconducting On-Chip Filter-Banks. *Journal of Low Temperature Physics*, 216(1-2), 144-153. <https://doi.org/10.1007/s10909-024-03118-w>

Important note

To cite this publication, please use the final published version (if applicable). Please check the document version above.

Copyright

Other than for strictly personal use, it is not permitted to download, forward or distribute the text or part of it, without the consent of the author(s) and/or copyright holder(s), unless the work is under an open content license such as Creative Commons.

Takedown policy

Please contact us and provide details if you believe this document breaches copyrights. We will remove access to the work immediately and investigate your claim.



Directional Filter Design and Simulation for Superconducting On-Chip Filter-Banks

Louis H. Marting^{1,2} · Kenichi Karatsu² · Akira Endo¹ · Jochem J. A. Baselmans^{1,2} · Alejandro Pascual Laguna^{1,2,3}

Received: 3 November 2023 / Accepted: 6 April 2024 / Published online: 4 May 2024
© The Author(s) 2024, corrected publication 2024

Abstract

Many superconducting on-chip filter-banks suffer from poor coupling to the detectors behind each filter. This is a problem intrinsic to the commonly used half-wavelength filter, which has a maximum theoretical coupling of 50 %. In this paper, we introduce a phase-coherent filter, called a directional filter, which has a theoretical coupling of 100 %. In order to study and compare different types of filter-banks, we first analyze the measured filter frequency scatter, losses, and spectral resolution of a DESHIMA 2.0 filter-bank chip. Based on measured fabrication tolerances and losses, we adapt the input parameters for our circuit simulations, quantitatively reproducing the measurements. We find that the frequency scatter is caused by nanometer-scale line width variations and that variances in the spectral resolution is caused by losses in the dielectric only. Finally, we include these realistic parameters in a full filter-bank model and simulate a wide range of spectral resolutions and oversampling values. For all cases, the directional filter-bank has significantly higher coupling to the detectors than the half-wave resonator filter-bank. The directional filter eliminates the need to use oversampling as a method to improve the total efficiency, instead capturing nearly all the power remaining after dielectric losses.

Keywords MKID · Spectrometer · Band-pass filter · Directional filter · Filter-bank

1 Introduction

On-chip superconducting filter-bank spectrometers are a promising technology for wideband spectroscopic observations in the (sub-)millimeter wavelength range [1–3]. However, the efficiency of current on-chip filter-banks is poor. Partly this is due to dielectric loss in the filters, but more fundamentally the current designs based on shunted half-wave resonator filters have a maximum theoretical coupling to the detector behind each filter of 50% [4–6]. Here, we introduce a phase-coherent filter,

Extended author information available on the last page of the article

called a directional filter, as an alternative filter design that ideally has an efficiency of 100%.

We model the performance of a directional filter numerically and compare it to the standard shunted half-wave resonator. This is done for an individual filter and for a full filter-bank. Additionally, we study the effects of fabrication tolerances and dielectric losses for a filter-bank with a spectral resolution of $R = f_0/\Delta f_0 = 500$ in a frequency band of 220–440 GHz, which is the target design for the DESHIMA 2.0 instrument [7], soon to be fielded to the ASTE telescope in Chile. In our model, we use the measured losses as well as the measured variations in losses and resonance frequency of the DESHIMA 2.0 filter-bank as input. Finally, a comparison is made between filter-banks using either directional filters or half-wave resonator filters for a variety of spectral resolutions and oversampling values.

In Sect. 2, we introduce the directional filter and show its performance. In Sect. 3, we show the results of simulations of a filter-bank model with ideal components. In Sect. 4, we introduce fabrication tolerances and dielectric loss. In Sect. 5, we study these tolerances and losses in realistic filter-banks across a range of spectral resolutions and oversampling values with full filter-bank simulations.

2 Directional Filter

A directional filter [8–12] is a symmetric four-port device that acts as a channel separating filter. Directional filters are characterized by four basic properties [8]: (1) they have four ports, one of which is always isolated from the input port; (2) the input power is filtered to one port with a band-pass response, while the remaining power emerges from another port with a complementary band-stop response; (3) the input port is non-reflecting when the other ports are impedance-matched; (4) these properties apply no matter which of the four ports is used.

A schematic of a directional filter, which consists of two half-wave resonators capacitively coupled to transmission lines at the top and bottom, is shown in the left panel of Fig. 1. The half-wave resonators are separated by a quarter wavelength at the top and by three-quarter wavelengths at the bottom. By making port 1 be the input: port 2 gives a band-stop response; port 3 has a band-pass response; and port 4 is isolated. In this configuration, the top transmission line, which we call the signal line, carries the wideband input signal captured by a broadband antenna. This configuration is as easily fabricated as two half-wave resonators next to each other. The only additional requirements are that there is enough room for each coupler and that the bottom transmission line has a meander to create the additional half-wavelength. Both conditions are easily satisfied.

The bottom transmission line is part of the microwave kinetic inductance detector (MKID), where the sub-millimeter radiation is absorbed and detected. The quarter wavelength and three-quarter wavelength sections could be swapped without changing the function of the directional filter due to the symmetry of the structure. This configuration is chosen to reduce the signal line length, and thus its loss. Daisy-chaining ports 1 and 2 of separately tuned filters creates a filter-bank, as we shall do in Sect. 3.

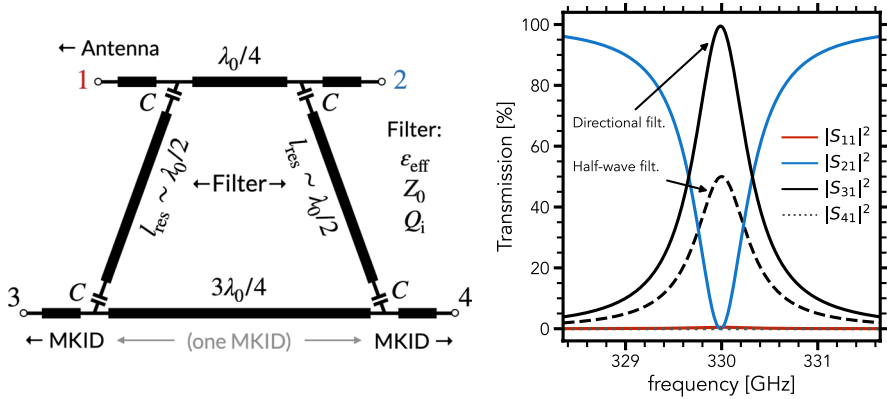


Fig. 1 A lossless directional filter with resonance frequency f_0 at 330 GHz. The circuit schematic is shown on the left. The bottom transmission line is part of the MKID detector, for details we refer to the text. On the right, the filter S-parameters around the resonance frequency are shown. The numerical response is calculated by building a circuit model similar to Pascual Laguna et al. [4]

The right panel of Fig. 1 shows the numeric response of the directional filter around its resonance, for comparison the $|S_{31}|^2$ for a half-wave resonator filter is also given. Shunted half-wave resonator filters cause an impedance mismatch on-resonance, which results in a theoretical transmission limit of 50% to the detector behind each filter. The directional filter overcomes this limit by matching the incoming and outgoing signal using a phase-coherent structure. The maximum on-resonance transmission of an ideal directional filter is instead 100%.

To absorb the power in the aluminum (Al) section of a $\lambda/4$ niobium titanium nitride (NbTiN)/Al hybrid MKID [13], we integrate the hybrid section of the MKID with the bottom of the coherent filter circuit by coupling co-planar waveguide (CPW) lines with an Al central line to ports 3 and 4. These must have sufficient length to absorb all power in the Al central line. In this case, both ports 3 and 4 see the characteristic impedance of the line, allowing to match both ports. This satisfies the third basic property of a directional filter. The hybrid CPW line to be connected to port 4 is in series with a wide NbTiN CPW section which is parallel-coupled to the microwave readout line. The equally long hybrid CPW MKID section to be connected to port 3 is short-circuited to ground to set the other boundary condition establishing the $\lambda/4$ microwave resonance of the MKID.

3 Filter-Bank Model

We will now discuss the performance of a filter-bank consisting of directional filters using a numerical model based on the model developed by Pascual Laguna et al. [4]. For the filter-bank model, we use ideal components and a filter overlap at 50% of the peak response. The target design is a spectral resolution of $R = f_0/\Delta f_0 = 500$ in a 220–440 GHz band, which is the target design for the DESHIMA 2.0 instrument

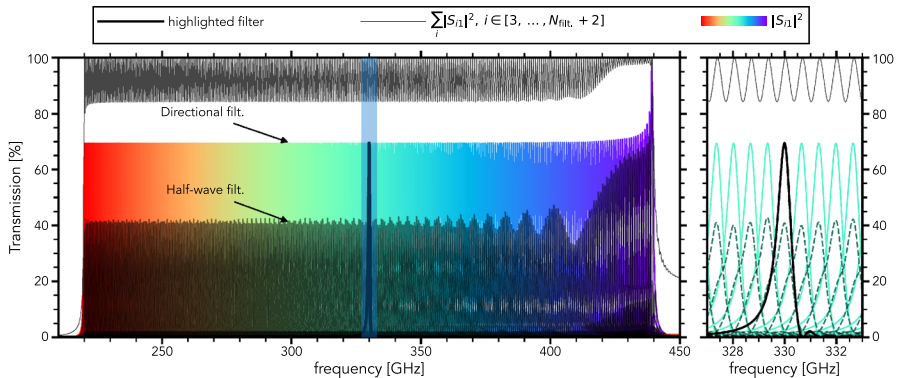


Fig. 2 Response of a lossless filter-bank with directional filters (solid lines) and half-wave resonator filters (dashed lines). Color lines indicate the response of each channel. The thin black line indicates the total power absorbed by the directional filter-bank. The thick black line highlights an individual filter

[7]. This configuration is a choice and other configurations are also possible [14], but we present our results in the most general way possible.

Figure 2 shows the spectral response of a lossless filter-bank consisting of directional filters. Across the filter-bank operating band, the total aggregate power captured by all channels varies from 85 to 100%, being maximum at the resonance frequency of each individual filter. The average peak response of individual filters is around 70%. Comparatively, the peak response of half-wave resonator filters is only 40%. Hence, the directional filter is almost twice as efficient in a filter-bank configuration compared to a half-wave resonator filter under ideal conditions (lossless and nominal design parameters) and no oversampling. Oversampling is defined as the ratio of the full-width half-maximum channel width over the channel resonance frequency separation, $\Delta f_i / (f_i - f_{i-1})$.

The highest frequency filter, which is first in the signal line from the antenna, shows the 100% efficiency that we expect from the single filter model. The other filters settle at an efficiency of 70%. This is a direct result of the 50% overlap design choice (oversampling = 1), where the tails of neighboring filters absorb the remaining 30%. This is further evidenced by the asymmetry of the filter shape in the zoom-in in Fig. 2 and by the 100% of the *total* power being absorbed ($\sum_i |S_{i1}|^2$, $i \in [3, \dots, N_{\text{filt.}} + 2]$) at each filter's resonance frequency. It shows that power at those frequencies is neither reflected at the filter-bank input port nor dissipated at the load terminating the signal line. Even at the intersection between adjacent filters, the total power coupled is 85%, significantly more than the value of 60% reported for the half-wave resonator filter (see Pascual Laguna [15], Fig. 3.7).

4 Tolerance Analysis

Using data from a half-wave resonator filter-bank for DESHIMA 2.0, we can include representative fabrication tolerances and dielectric losses in the filter-bank model. The blue data in Fig. 3 show these variances measured in the resonance

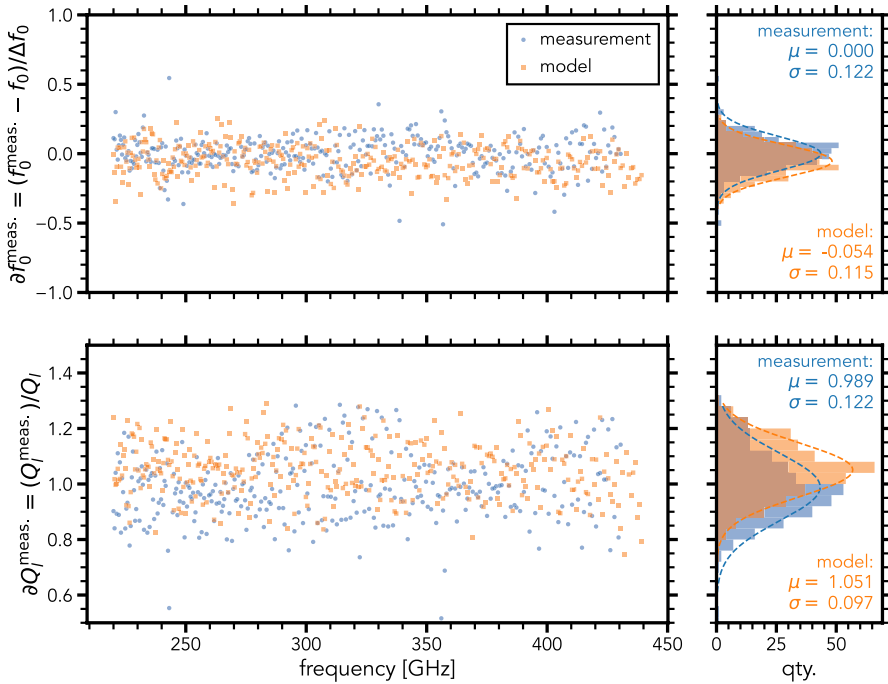


Fig. 3 Normalized scatter of $\partial Q_1^{\text{meas.}}$ and $\partial f_0^{\text{meas.}}$ for a DESHIMA 2.0 chip with design values $Q_1 = 500$ and $f_0 = 220\text{--}440$ GHz. $\Delta f_0 = f_0 / Q_1$. The blue points indicate the measured data, the orange points indicate our model results, we refer to the text for details. The offsets in the measurements have been normalized to only show scatter

frequency f_0 and loaded quality factor Q_1 for the DESHIMA 2.0 chip. The loaded quality factor Q_1 is equal to the spectral resolution $R = f_0 / \Delta f_0$, i.e., an oversampling value of 1. The normalized f_0 scatter is defined as: $\partial f_0^{\text{meas.}} = (f_0^{\text{meas.}} - f_0) / \Delta f_0$. The normalized Q_1 scatter is defined as: $\partial Q_1^{\text{meas.}} = (Q_1^{\text{meas.}}) / Q_1$. The first step in our analysis is to find which parameters in our model are responsible for the observed scatter in f_0 and Q_1 .

Each resonator in the directional filter model in Fig. 1 has five input parameters, namely l_{res} , ϵ_{eff} , C , Z_0 and Q_i . Two parameters vary for each resonator in our filter-bank design: l_{res} is the resonator length; and C is the coupling capacitance. They are used to set the resonance frequency f_0 and coupling quality factor Q_c . The other parameters, ϵ_{eff} , Z_0 and Q_i , define the resonator transmission line and are given by its cross-sectional dimensions and the material properties. They ideally stay constant across the filter-bank.

By taking a single resonator and varying each of these parameters slightly, we can find how strongly each of them affects f_0 and Q_1 . In turn, we can model with SONNET how strongly each of these parameters is affected by realistic fabrication tolerances. The result, reported in Table 1, is a set of model input parameters with their sensitivities mapped and linked to various underlying fabrication errors. The table gives the deviation for each parameter required to create a change in Q_1 or f_0

of 12% for a single resonator, which is the measured variance in DESHIMA 2.0 (see Fig. 3).

It should be noted that the parameters are affected by multiple causes (e.g., variations in gap width of the couplers, line width, thickness of the materials), which were all investigated. However, only the most sensitive cause affecting the parameters is reported.

From Table 1, we can conclude that the scatter in Q_1 can *only* be explained by Q_i scatter as any other parameter causes a scatter in f_0 well exceeding the measured value in DESHIMA 2.0. To understand why Q_i scatter affects Q_1 so much, consider the following equation:

$$\frac{1}{Q_1} = \frac{2}{Q_c} + \frac{1}{Q_i}. \quad (1)$$

This equation gives Q_1 in terms of Q_c and Q_i , assuming two equal couplers on each end of the resonator (hence the factor 2). From 1, it is clear that the sensitivity of Q_1 to Q_i largely depends on the ratio between Q_c and Q_i . If Q_i is relatively small compared to Q_c , any variance on it will have a large impact on Q_1 . The average measured Q_i of this chip is approximately 1200, which is close to the Q_c values of the measured chip.

The frequency scatter is most likely caused by a variance in Z_0 , caused by nanometer-scale line width variations from filter to filter. This corresponds to the beam step size used for our electron-beam lithography step that defines these features.

Applying a variance to our model using only the bold parameters in Table 1 results in an f_0 and Q_1 scatter given by the orange data of Fig. 3. The model and measurement distributions are in excellent agreement, showing we can accurately model the fabrication errors.

5 Full Filter-Bank Simulations

We now simulate realistic filter-banks across a range of spectral resolutions and oversampling values, and we compare the directional filter against the half-wave resonator filter. The realistic losses ($Q_i = 1200$) and fabrication errors (bold parameters

Table 1 Mapping of our model parameters to fabrication errors

Parameter	Cause	$\partial f_0^{\text{meas.}} = 12\%$	$\partial Q_1^{\text{meas.}} = 12\%$
l_{res}	Length	42 nm	17.7 μm
ϵ_{eff}	$R_s \rightarrow L_k$	0.2 p Ω/\square	113 p Ω/\square
C	Gap width	5.5 nm	20–60 nm
Z_0	Line width	1 nm^a	
Q_i	Dielectric loss		23.4%

The last two columns give the error needed to achieve the offset in the column heading. The offset corresponds to the normalized variance of the measured DESHIMA 2.0 data in Fig. 3. The bold parameters are used to add variances to the model. An empty value means that the parameter has no influence on that variance

^a 1 nm corresponds to a variance of $\partial Z_0/Z_0 = 1.2\%$ in our model

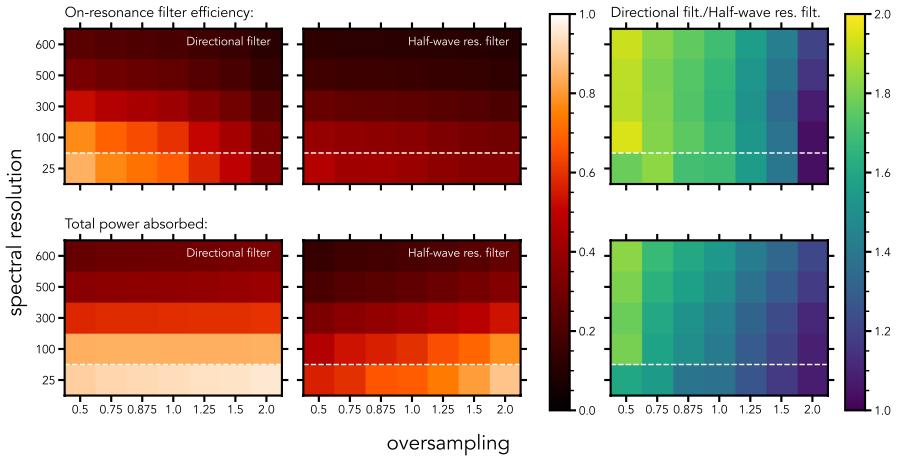


Fig. 4 Simulations of realistic filter-banks (using the variations of the bold parameters in Table 1) across a range of spectral resolutions and oversampling values, using $Q_i = 1200$. The median values of both the on-resonance filter efficiency and the total power absorbed (also on-resonance) for each filter configuration are shown in the graph. The relative advantage of the directional filter is shown on the right

in Table 1) are incorporated in this simulation. We note that in case of the directional filter, the Q_i and the Z_0 variance are applied independently to both resonators. Fig. 4 shows the results. The left-most column in each figure shows the near-isolated performance of both filter types for a range of spectral resolutions, since the undersampled filter-bank spaces the filters far apart in the spectrum. The bottom row is the case where fabrication tolerances and losses hardly matter due to the low spectral resolution; hence, these can be seen as an ideal case with no scatter and no losses in the materials.

Figure 4 shows that the directional filter outperforms the half-wave resonator filter, even with realistic losses and fabrication errors. From the rightmost panels in Fig. 4 it is clear that, for a given oversampling value, the performance ratio remains similar between the directional filter and the half-wave resonator filter going from a spectral resolution of 25, representing an ideal filter-bank without fabrication defects, to higher spectral resolutions, representing a realistic case. In terms of on-resonance filter efficiency, the directional filter is close to being twice as efficient as the half-wave resonator filter for all spectral resolutions, showing that dielectric losses affect both filter types equally. Additionally, we can see the effect of the limited Q_i deteriorating the filter-bank performances in all cases for spectral resolutions above 100.

Only at high oversampling values does the median on-resonance filter efficiency of the directional filter converge to the efficiency of the half-wave resonator filter. At this point, the filters are spectrally spaced so closely that the tails of neighboring filters are absorbing a significant amount of the power on-resonance. However, even at the highest oversampling presented, the total power absorbed by the directional filter is still greater than that of the half-wave resonator filter. This means that even if

one wants to sum the outputs of multiple filters to improve the total absorption, the directional filter configuration still remains the best choice.

Furthermore, the total power absorbed is near independent of oversampling for the directional filter. This means that the directional filter eliminates the need to oversample and sum outputs altogether [14]. The directional filter captures nearly all the power available after dielectric losses are accounted for, and it is the most efficient that any transmission line resonator filter can be.

6 Conclusion

We have introduced a phase-coherent filter, called a directional filter, as an alternative to the widely used shunted half-wave resonator filter for superconducting on-chip filter-banks. The directional filter overcomes the maximum pass-band response limit of 50% for a half-wave resonator filter, with an efficiency of 100% in a lossless scenario. This is achieved by matching the incoming and outgoing signals using a phase-coherent structure comprising two half-wave resonators. In a filter-bank configuration, the directional filter retains its advantage and has a nearly two times better efficiency compared to the half-wave resonator filter-bank.

Fabrication errors and dielectric losses are added to our model based on measurements from DESHIMA 2.0. We found that the frequency scatter is mainly caused by variations in the resonator characteristic impedance Z_0 due to nanometer-scale line width variations. We also found that the loaded quality factor Q_l scatter can only be caused by internal quality factor Q_i (dielectric loss) variations.

We can accurately represent a realistically fabricated filter-bank by incorporating these fabrication errors and dielectric losses for both filter types. Comparing these realistic filter-banks across a range of oversampling values and spectral resolutions shows that the directional filter performs better in all cases.

Acknowledgements The authors thank D.J. Thoen and L.G.G. Olde Scholtenhuis for their useful discussions on nanometer-scale line width variations in e-beam lithography. This work is supported by the European Union (ERC Consolidator Grant No. 101043486 TIFUUN). Views and opinions expressed are however those of the authors only and do not necessarily reflect those of the European Union or the European Research Council Executive Agency. Neither the European Union nor the granting authority can be held responsible for them.

Author Contributions A.P.L. introduced the directional filter concept for use in an sub-mm on-chip filter-bank. K.K. measured the DESHIMA 2.0 chip. J.J.A.B. and A.E. are the PhD supervisors of L.H.M. and helped with the conclusions and analysis. The numerical filter-bank model was developed by A.P.L. and further improved upon by L.H.M. L.H.M. performed the tolerance analysis and simulations. L.H.M. wrote the main manuscript text. L.H.M. prepared all figures and tables. All authors reviewed the manuscript.

Declarations

Conflict of interest This work is supported by the European Union (ERC Consolidator Grant No. 101043486 TIFUUN). Views and opinions expressed are however those of the authors only and do not necessarily reflect those of the European Union or the European Research Council Executive Agency. Neither the European Union nor the granting authority can be held responsible for them.

Open Access This article is licensed under a Creative Commons Attribution 4.0 International License, which permits use, sharing, adaptation, distribution and reproduction in any medium or format, as long as you give appropriate credit to the original author(s) and the source, provide a link to the Creative Commons licence, and indicate if changes were made. The images or other third party material in this article are included in the article's Creative Commons licence, unless indicated otherwise in a credit line to the material. If material is not included in the article's Creative Commons licence and your intended use is not permitted by statutory regulation or exceeds the permitted use, you will need to obtain permission directly from the copyright holder. To view a copy of this licence, visit <http://creativecommons.org/licenses/by/4.0/>.

References

1. A. Endo, K. Karatsu, Y. Tamura, T. Oshima, A. Taniguchi, T. Takekoshi, S. Asayama, T.J.L.C. Bakx, S. Bosma, J. Bueno, K.W. Chin, Y. Fujii, K. Fujita, R. Huiting, S. Ikarashi, T. Ishida, S. Ishii, R. Kawabe, T.M. Klapwijk, K. Kohno, A. Kouchi, N. Llombart, J. Maekawa, V. Murugesan, S. Nakatsubo, M. Naruse, K. Ohtawara, A. Pascual Laguna, J. Suzuki, K. Suzuki, D.J. Thoen, T. Tsukagoshi, T. Ueda, P.J. de Visser, P.P. van der Werf, S.J.C. Yates, Y. Yoshimura, O. Yurduseven, J.J.A. Baselmans, First light demonstration of the integrated superconducting spectrometer. *Nat. Astron.* **3**(11), 989–996 (2019). <https://doi.org/10.1038/s41550-019-0850-8>
2. J. Redford, P.S. Barry, C.M. Bradford, S. Chapman, J. Glenn, S. Hailey-Dunsheath, R.M.J. Janssen, K.S. Karkare, H.G. LeDuc, P. Mauskopf, R. McGeehan, E. Shirokoff, J. Wheeler, J. Zmuidzinas, SuperSpec: on-chip spectrometer design, characterization, and performance. *J. Low Temp. Phys.* **209**(3), 548–555 (2022). <https://doi.org/10.1007/s10909-022-02866-x>
3. G. Cataldo, E.M. Barrentine, B.T. Bulcha, N. Ehsan, L.A. Hess, O. Noroozian, T.R. Stevenson, E.J. Wollack, S.H. Moseley, E.R. Switzer, Second-generation micro-spec: a compact spectrometer for far-infrared and submillimeter space missions. *Acta Astronaut.* **162**, 155–159 (2019). <https://doi.org/10.1016/j.actaastro.2019.06.012>
4. A. Pascual Laguna, K. Karatsu, D.J. Thoen, V. Murugesan, B.T. Buijtenorp, A. Endo, J.J.A. Baselmans, Terahertz band-pass filters for wideband superconducting on-chip filter-bank spectrometers. *IEEE Trans. Terahertz Sci. Technol.* **11**(6), 635–646 (2021). <https://doi.org/10.1109/TTHz.2021.3095429>
5. A. Kovács, P.S. Barry, C.M. Bradford, G. Chattopadhyay, P. Day, S. Doyle, S. Hailey-Dunsheath, M. Hollister, C. McKenney, H.G. LeDuc, N. Llombart, D.P. Marrone, P. Mauskopf, R.C. O'Brien, S. Padin, L.J. Swenson, J. Zmuidzinas, SuperSpec: Design concept and circuit simulations, in *Millimeter, Submillimeter, and Far-Infrared Detectors and Instrumentation For Astronomy VI*, vol 8452 (2012), pp. 748–757. <https://doi.org/10.1117/12.927160>
6. A. Endo, P. van der Werf, R.M.J. Janssen, P.J. de Visser, T.M. Klapwijk, J.J.A. Baselmans, L. Ferrari, A.M. Baryshev, S.J.C. Yates, Design of an integrated filterbank for DESHIMA: on-chip submillimeter imaging spectrograph based on superconducting resonators. *J. Low Temp. Phys.* **167**(3), 341–346 (2012). <https://doi.org/10.1007/s10909-012-0502-1>
7. A. Taniguchi, T.J.L.C. Bakx, J.J.A. Baselmans, R. Huiting, K. Karatsu, N. Llombart, M. Rybak, T. Takekoshi, Y. Tamura, H. Akamatsu, S. Brackenhoff, J. Bueno, B.T. Buijtenorp, S.O. Dabironzare, A.-K. Doing, Y. Fujii, K. Fujita, M. Gouwerok, S. Hähnle, T. Ishida, S. Ishii, R. Kawabe, T. Kitayama, K. Kohno, A. Kouchi, J. Maekawa, K. Matsuda, V. Murugesan, S. Nakatsubo, T. Oshima, A. Pascual Laguna, D.J. Thoen, P.P. van der Werf, S.J.C. Yates, A. Endo, DESHIMA 2.0: development of an integrated superconducting spectrometer for science-grade astronomical observations. *J. Low Temp. Phys.* **209**(3), 278–286 (2022). <https://doi.org/10.1007/s10909-022-02888-5>
8. S.B. Cohn, F.S. Coale, Directional channel-separation filters. *Proc. IRE* **44**(8), 1018–1024 (1956). <https://doi.org/10.1109/JRPROC.1956.275043>
9. F.S. Coale, A traveling-wave directional filter. *IRE Trans. Microw. Theory Tech.* **4**(4), 256–260 (1956). <https://doi.org/10.1109/TMTT.1956.1125073>
10. B.M. Oliver, Directional electromagnetic couplers. *Proc. IRE* **42**(11), 1686–1692 (1954). <https://doi.org/10.1109/JRPROC.1954.274664>
11. E.M.T. Jones, Coupled-strip-transmission-line filters and directional couplers. *IRE Trans. Microw. Theory Tech.* **4**(2), 75–81 (1956). <https://doi.org/10.1109/TMTT.1956.1125022>

12. L.P. Tuttle, R.D. Wanselow, Practical design of strip-transmission-line half-wavelength resonator directional filters. *IRE Trans. Microw. Theory Tech.* **7**(1), 168–173 (1959). <https://doi.org/10.1109/TMTT.1959.1124642>
13. R.M.J. Janssen, J.J.A. Baselmans, A. Endo, L. Ferrari, S.J.C. Yates, A.M. Baryshev, T.M. Klapwijk, High optical efficiency and photon noise limited sensitivity of microwave kinetic inductance detectors using phase readout. *Appl. Phys. Lett.* **103**(20), 203503 (2013). <https://doi.org/10.1063/1.4829657>
14. S. Hailey-Dunsheath, E. Shirokoff, P.S. Barry, C.M. Bradford, G. Chattopadhyay, P. Day, S. Doyle, M. Hollister, A. Kovacs, H.G. LeDuc, P. Mauskopf, C.M. McKenney, R. Monroe, R. O'Brient, S. Padin, T. Reck, L. Swenson, C.E. Tucker, J. Zmuidzinas, Status of SuperSpec: a broadband, on-chip millimeter-wave spectrometer, in *Millimeter, Submillimeter, and Far-Infrared Detectors and Instrumentation for Astronomy VII*, vol 9153 (2014), pp. 181–196. <https://doi.org/10.1117/12.2057229>
15. A. Pascual Laguna, On-chip solutions for future THz imaging spectrometers. PhD thesis, Delft University of Technology (2022). <https://doi.org/10.4233/uuid:512da833-dc9d-4301-b566-35243d2f1f9b>

Authors and Affiliations

Louis H. Marting^{1,2} · Kenichi Karatsu² · Akira Endo¹ · Jochem J. A. Baselmans^{1,2} · Alejandro Pascual Laguna^{1,2,3}

✉ Louis H. Marting
l.h.marting@tudelft.nl

Kenichi Karatsu
k.karatsu@tudelft.nl

Akira Endo
a.endo@tudelft.nl

Jochem J. A. Baselmans
j.baselmans@sron.nl

Alejandro Pascual Laguna
alejandro.pascual@cab.inta-csic.es

¹ Faculty of Electrical Engineering, Mathematics and Computer Science, Delft University of Technology, Mekelweg 4, 2628 CD Delft, Zuid-Holland, The Netherlands

² SRON–Netherlands Institute for Space Research, Niels Bohrweg 4, 2333 CA Leiden, Zuid-Holland, The Netherlands

³ Centro de Astrobiología, CSIC-INTA, 28850 Torrejón de Ardoz, Madrid, Spain